

THE THREE-DIMENSIONAL STRUCTURES IN TURBULENT COUETTE-POISEUILLE FLOWS ON THE VERGE OF SEPARATION

Zehuan Wu, Callum Atkinson, Julio Soria

Laboratory for Turbulence Research in Aerospace and Combustion
 Department of Mechanical and Aerospace Engineering
 Monash University

Clayton, Victoria 3800, Australia

zehuan.wu@monash.edu, callum.atkinson@monash.edu, julio.soria@monash.edu

Atsushi Sekimoto

Department of Materials Engineering Science
 Osaka University

Osaka 560-8531, Japan

asekimoto@cheng.es.osaka-u.ac.jp

ABSTRACT

This work investigates flow structures in Couette-Poiseuille (C-P) flows with the adverse pressure gradient (APG) adjusted to create zero mean skin friction on the stationary wall. The vortical structures are identified as regions with a positive value of the discriminant of the velocity gradient tensor (Chong *et al.*, 1990; Soria *et al.*, 1994). The data used in current study are from direct numerical simulation (DNS). The enstrophy density and the dissipation of kinetic energy carried by flow structures are instigated by examining the second invariants of the symmetric strain rate tensor S_{ij} and the skew-symmetric rate of rotation tensor W_{ij} (Chong *et al.* (1998)). Some characterizations of the topological flow structures in the near-wall region are similar to a viscous sub-layer in channel flows (Blackburn *et al.*, 1996).

INTRODUCTION

Understanding flow structure of a turbulent flow as it approaches separation is essential for separation control. The topological classification of the velocity gradient, rate-of-strain and rate-of-rotation tensors is first employed to study the turbulent mixing layer by Soria *et al.* (1994). The invariants can be used to depict the stretching and rotation of eddies in turbulent flows and they have been studied in a wide range of flow configurations, such as turbulent boundary layers with APG or zero pressure gradient (ZPG)(Chong *et al.*, 1998), turbulent channel flows (Sekimoto *et al.*, 2016b; Blackburn *et al.*, 1996) and the turbulent/nonturbulent interface in jets (da Silva & Pereira, 2008). Also, important features are obtained by analyzing the volume integral of the invariants especially in homogeneous flows (Soria *et al.*, 1997). These studies regarding the properties of the velocity gradient tensors showed a number of common features of flow motions. In the buffer layer, log layer and wake region in wall-bounded turbulent flows, the joint probability density function of R and Q features a tear-drop shape, indicating the similar proportion of vortical

structures and saddles.

In this paper, we examine the distributions of the invariants of the velocity gradient tensor A_{ij} , the rate of strain tensor S_{ij} and the rate of rotation tensor W_{ij} across the shearless wall to half channel height in the C-P flow in order to clarify the topology of the turbulent flow structures when the flow is on the verge of separation.

NUMERICAL METHOD

Governing equations in direct numerical simulations

In the DNS, the streamwise, wall-normal and spanwise directions are x , y and z respectively. The corresponding velocity components are u , v and w . $\langle \rangle_{xz}$ represents time-dependent average in x and z which are homogeneous directions. Capital letters, such as U , represent mean values over all homogeneous directions and time. Primes, such as u' , are fluctuations. Lower letters, such as u , represent instantaneous values, so $u = U + u'$. The sketch of the C-P flow is shown in figure 1. In the DNS, the Navier-Stokes equations for incompressible flow are solved in the form of evolution equations for the wall-normal vorticity ω_y and the Laplacian of the wall-normal velocity $\phi = \nabla^2 v$ (Kim *et al.*, 1987),

$$\frac{\partial \omega_y}{\partial t} + U \frac{\partial \omega_y}{\partial x} = h_g + \nu \nabla^2 \omega_y \quad (1)$$

$$\frac{\partial \phi}{\partial t} + U \frac{\partial \phi}{\partial x} = h_v + \nu \nabla^2 \phi \quad (2)$$

where ν is the kinematic viscosity, with h_g and h_v defined as

$$h_g = \frac{\partial(H_x)}{\partial z} - \frac{\partial H_z}{\partial x} - \frac{dU}{dy} \frac{\partial v}{\partial z} \quad (3)$$

$$h_v = -\frac{\partial}{\partial y} \left(\frac{\partial H_x}{\partial x} + \frac{\partial H_z}{\partial z} \right) + \left(\frac{\partial^2}{\partial x^2} + \frac{\partial^2}{\partial z^2} \right) H_y \quad (4)$$

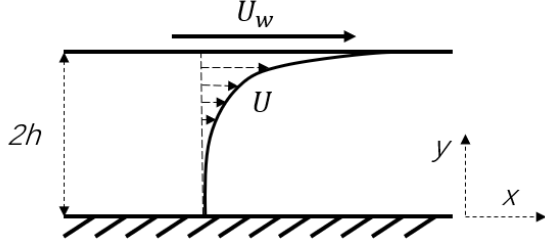


Figure 1. Sketch of mean velocity profiles and flow configuration.

where $(H_x, H_y, H_z) = (u, v, w) \times (\omega_x, \omega_y, \omega_z)$.

The governing equations for $\langle u \rangle_{xz}$ and $\langle w \rangle_{xz}$ are

$$\frac{\partial \langle u \rangle_{xz}}{\partial t} = -\frac{\partial \langle uv \rangle_{xz}}{\partial y} + \nu \frac{\partial^2 \langle u \rangle_{xz}}{\partial y^2} \quad (5)$$

$$\frac{\partial \langle w \rangle_{xz}}{\partial t} = -\frac{\partial \langle wv \rangle_{xz}}{\partial y} + \nu \frac{\partial^2 \langle w \rangle_{xz}}{\partial y^2} \quad (6)$$

since the flow is homogeneous in x and z , $\langle v \rangle_{xz} = 0$ because of the continuity. These equations are solved using the spectral method, which uses Fourier series in the streamwise and spanwise directions and Chebychev polynomial in the wall-normal direction (Sekimoto *et al.*, 2016a, 2018). In the simulation, the computational domain is periodic in x and z . L_x , L_y and L_z are the size of the domain in the streamwise, wall-normal and spanwise directions respectively, such that $0 \leq x \leq L_x$ and $0 \leq z \leq L_z$. In streamwise and spanwise directions, two-dimensional Fourier-expansions with 3/2 dealiasing are used. The grid numbers in physical space are N_x and N_z . The corresponding resolution are $\Delta x = L_x/N_x$ and $\Delta z = L_z/N_z$. In the wall-normal direction, Chebychev polynomial is used. Time stepping is carried out by a third-order Runge-Kutta method which is described in detail in Sekimoto *et al.* (2016a).

In this paper, we present a simulation with the Reynolds number, $Re = 2880$, defined by the half channel height, h , and the velocity of the moving wall, U_w . The DNS parameters are summarised in table 1. Δx^+ and Δz^+ are the grid spacing Δx and Δz in viscous length scale defined in terms of the friction velocity u_τ at the moving wall and the kinematic viscosity ν . y_{10}^+ is the distance of the 10th grid from the wall in viscous length scale. β represents the non-dimensional pressure gradient, $\beta = hH/\tau$, where H is the pressure gradient and τ is the mean wall shear stress at the stationary wall.

Velocity gradient invariants

The velocity gradient tensor is defined as $A_{ij} = \partial u_i / \partial x_j$. The characteristic equation of A_{ij} is given by

$$\lambda^3 + P\lambda^2 + Q\lambda + R = 0 \quad (7)$$

where P , Q and R are the first, second and third invariants respectively, defined as

$$P = -\text{tr}(A) \quad (8)$$

$$Q = \frac{1}{2}(P^2 - \text{tr}(A^2)) \quad (9)$$

$$R = -\det(A) \quad (10)$$

where $\text{tr}()$ is the trace and the $\det()$ means the determinant of the tensor. Due to the continuity, P is zero for incompressible flows. The discriminant of the velocity gradient tensor is given by

$$D = \frac{27}{4}R^2 + Q^3 \quad (11)$$

The velocity gradient tensor can be decomposed into two parts, the rate of strain tensor S_{ij}

$$S_{ij} = \frac{1}{2}(A_{ij} + A_{ji}) \quad (12)$$

and the rate of rotation tensor W_{ij}

$$W_{ij} = \frac{1}{2}(A_{ij} - A_{ji}) \quad (13)$$

In addition, the invariants of S_{ij} are P_s , Q_s and R_s which are defined in a similar way as the invariants of A_{ij} . Q_s is proportional to the local rate of viscous dissipation of kinetic energy $\varepsilon = 2\nu S_{ij}S_{ij} = -4\nu Q_s$. For incompressible flow, $P_s = 0$.

The invariants of W_{ij} are P_w , Q_w and R_w . $P_w = R_w = 0$ for incompressible flows. $Q_w = \frac{1}{2}W_{ij}W_{ij}$ is related with the enstrophy density.

RESULTS

One-point statistics

The mean streamwise velocity profile normalized by U_w is shown in figure 2. In outer scaling, we can see the feature of the mean velocity distribution clearly in the region far away from the wall. At the stationary bottom wall where $y/h = 0$, the gradient of mean streamwise velocity is negligible compared with on the moving top wall where $y/h = 2$. The local shear stress increases monotonically and reaches its maximum at the moving wall. The shearless region cannot be seen clearly in outer scalings so the mean streamwise velocity normalized by u_H and l_H is shown in figure 3. The characteristic velocity and length, u_H and l_H , were first used by (Stratford, 1959) in the study of a separating turbulent boundary layer. u_H and l_H are defined as follows:

$$u_H = \left(-\frac{\nu}{\rho}H\right)^{1/3} \quad (14)$$

$$l_H = \nu/u_H \quad (15)$$

where ρ is the density of the fluid and H is the pressure gradient. In this paper, u_H and l_H will be referred to as Stratford units for simplicity.

We can see that the shearless region exits from $y/l_H = 0$ to 1 corresponding $y/h = 0$ to 0.033. The profile then follows a linear trend from $y/l_H = 1$ to 16 ($y/h = 0.033$ to 0.50) which is called the square-root layer. The study by

Table 1. Parameters of the simulation.

Re	L_x	L_y	L_z	N_x	N_y	N_z	Δx^+	Δz^+	y_{10}^+	β
2880	$8\pi h$	$2h$	$4\pi h$	1280	257	1024	5.3	3.3	2.0	-672

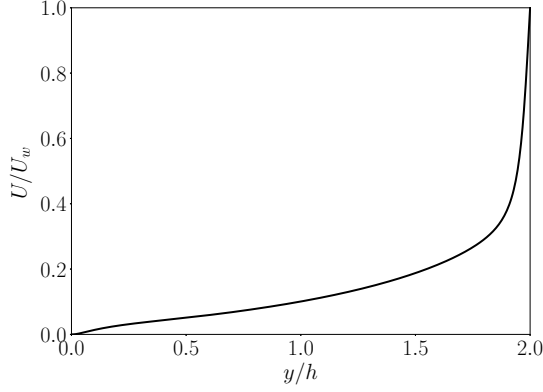


Figure 2. Profile of mean streamwise velocity U normalized by half channel height h and the velocity of the wall U_w .

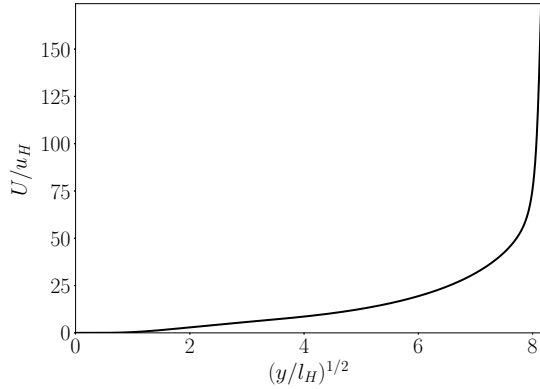


Figure 3. Profile of mean streamwise velocity U in Stratford units.

Coleman *et al.* (2017) showed that the range of the shearless region seems to be independent of the Reynolds number while the range of the square-root layer is not. At $y/l_H = 16$ to 32 ($y/h = 0.50$ to 1.0), the profile is no longer linear and more affected by the moving wall. Thus, in this paper, the structures are investigated in these three regions.

Figure 4 shows the streamwise, spanwise and wall-normal velocity fluctuations $\langle u'u' \rangle$, $\langle v'v' \rangle$, $\langle w'w' \rangle$ and Reynolds stress $\langle u'v' \rangle$ in Stratford units. It is shown that all the fluctuations remain approximately zero in the shearless region and then start to increase until they reach their respective maximum near the moving wall. It is worth noting that the wall-normal velocity fluctuation $\langle v'v' \rangle$ is linear in the square-root layer as shown in figure 4. The Reynolds stress $\langle u'v' \rangle$ is also linear with wall-normal distance in outer scaling (Figure 5).

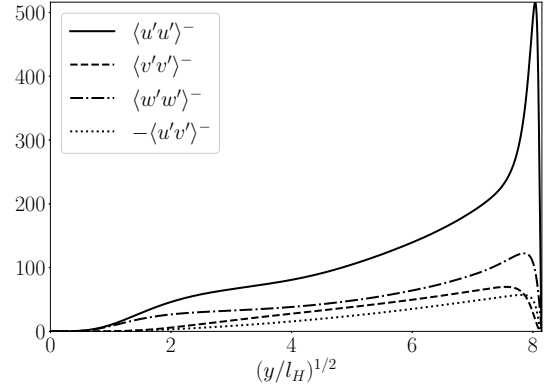


Figure 4. Profile of streamwise, wall-normal and spanwise velocity fluctuation and Reynolds stress in Stratford units. $\langle u'u' \rangle^- = \langle u'u' \rangle / (u_H)^2$, $\langle v'v' \rangle^- = \langle v'v' \rangle / (u_H)^2$, $\langle w'w' \rangle^- = \langle w'w' \rangle / (u_H)^2$ and $\langle u'v' \rangle^- = \langle u'v' \rangle / (u_H)^2$

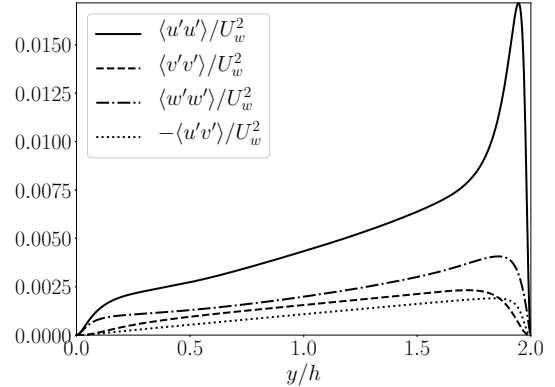


Figure 5. Profile of streamwise, wall-normal and spanwise velocity fluctuation and Reynolds stress in outer scaling.

Turbulent structures

All the invariants in Figure 6 to 8 are normalized by $\langle Q_w \rangle_V$ which is the space average of Q_w . As pointed out by Soria *et al.* (1997), $\langle Q_w \rangle_V = \langle -Q_s \rangle_V$ in homogeneous flows. Then it is better to normalize the invariants using a scaling related with the invariants themselves rather than outer scalings. The gray level are logarithmic in these figures.

Figure 6 shows the joint probability density function (JPDF) between Q and R in regions $0 < y/l_H < 1$, $1 < y/l_H < 16$ and $16 < y/l_H < 32$ separately. The blue line represents $D = 0$. No tear-drop shape can be observed in the region $0 < y/l_H < 1$. The contour lines correspond the probability of 0.98, 0.96 and 0.91. The JPDF has the smallest extent in the region $0 < y/l_H < 1$ due to the small ve-

locity gradients in that region. A preference for the third and fourth quadrants can be seen, indicating more saddle topologies in this region. This feature is similar to the viscous sub-layer in turbulent channel flows observed by Blackburn *et al.* (1996). Moving away from the wall, in regions $1 < y/l_H < 16$ and $16 < y/l_H < 32$, the preference for the second and fourth quadrants becomes apparent, showing the typical tear-drop shape found in turbulent boundary layers, indicating more stable stretching vortical structures (Chong *et al.*, 1998). The extent of the JPDF becomes larger which means it still does not reach the wake region otherwise the extent should decrease. The shape in the JPDF is similar to the buffer layer or log-law region in a turbulent channel flow (Blackburn *et al.*, 1996), indicating the viscous effect is negligible at $y/l_H > 1$. The contour lines in $1 < y/l_H < 16$ correspond the probability of 0.98, 0.96 and 0.88. In $16 < y/l_H < 32$, The contour lines correspond the probability of 0.96, 0.89 and 0.75. This shows that the invariants become more extended in range and have a trend of overall expansion.

Figure 7 shows the JPDF between Q_s and R_s in three regions. The influence of the shearless wall can be seen in the region $0 < y/l_H < 1$. The contour lines correspond the probability of 0.98, 0.93 and 0.85. The distribution of data are crowd along $R_s = 0$ and high negative Q_s . This indicates the highest dissipation of kinetic energy occurs in $0 < y/l_H < 1$. This preference is also similar to the viscous sub-layer in a turbulent channel flow (Blackburn *et al.*, 1996). With the distance from the wall increasing, the minimum value of Q_s decreases, the extent of R_s increases and a gathering towards $D_s = 0$ can be seen. This shows the rate of strain becomes more three-dimensional and local dissipation is much smaller compared with the region $0 < y/l_H < 1$. In the region $1 < y/l_H < 16$, the contour lines correspond the possibility 0.99, 0.97 and 0.92. In the region $16 < y/l_H < 32$, the contour lines correspond the possibility 0.98, 0.94 and 0.84. This implies that most of the data are located within a small region ($Q_s < -0.2$ and $0.1 < R_s < 0.1$), while only about 10% of them increase rapidly.

The JPDF between Q_s and Q_w in regions $0 < y/l_H < 1$, $1 < y/l_H < 16$ and $16 < y/l_H < 32$ is shown in figure 8. In the region $0 < y/l_H < 1$, all data follow a 45° line, which is similar to a viscous sub-layer in a turbulent channel flow (Blackburn *et al.*, 1996). In this region, Q_w and Q_s are balanced, which in turn indicates the negligible wall shear stress or velocity gradients. In the region $1 < y/l_H < 16$, the effect of the wall can still be observed due to the weak preference towards the 45° line, so the vortex sheet is still apparent and the contour lines correspond 0.99, 0.98 and 0.94. In the region $16 < y/l_H < 32$, a mix of all motion types happens due to more scattered distribution. The contour lines within this region correspond 0.99, 0.96 and 0.87. The distribution has a trend of moving to $Q_s = 0$, indicating more vortex tubes or filaments in the region.

CONCLUDING REMARKS

Direct numerical simulation of a Couette-Poiseuille (C-P) flows with zero mean skin friction on the stationary wall has been undertaken. One-point statistics of the flow are presented, the Reynolds stress is found to be linear with wall-normal coordinate from the shear-less wall. Due to zero mean wall shear stress, viscous units are not applicable. A regional division based on Stratford units is

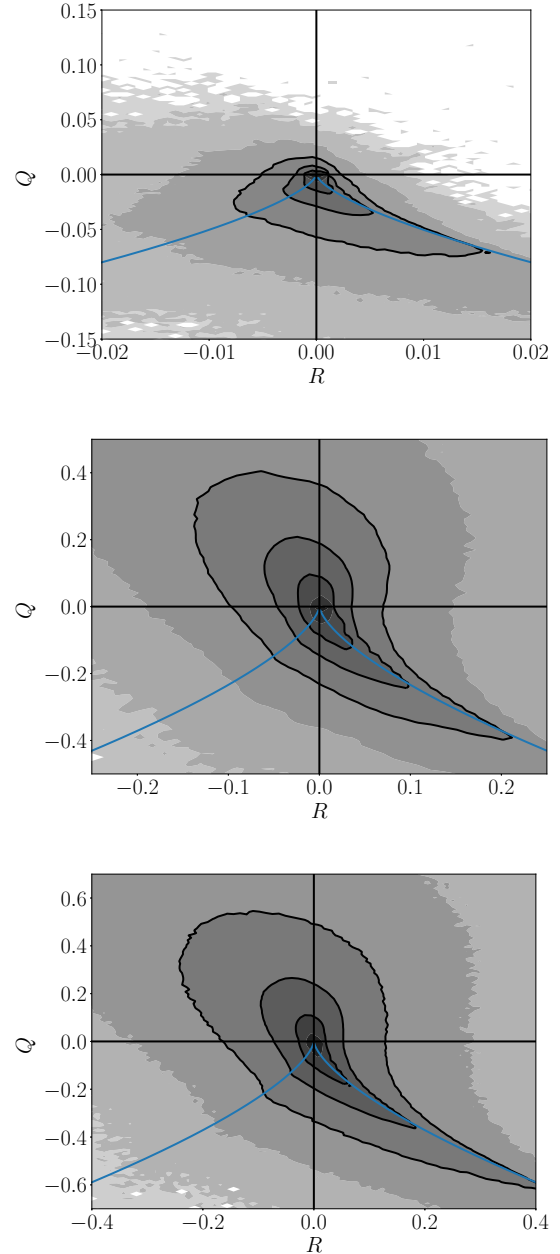


Figure 6. Joint Probability density function between Q and R normalized by $\langle Q_w \rangle_V$ in the regions $0 < y/l_H < 1$, $1 < y/l_H < 16$ and $16 < y/l_H < 32$.

proposed. The region $0 < y/l_H < 1$ seems to be independent with Re and the features of all the flow topologies are similar to a viscous sub-layer in a channel flow (Blackburn *et al.*, 1996). In the square root layer, $1 < y/l_H < 16$, the distribution of Q_w and Q_s represents a unique feature which is unlike any region in a turbulent boundary layer or channel flow. The joint p.d.f. in this region has a relative mixture of motion types due to the scattered distribution but also with a preference towards the 45° line. It seems like a transitional region. In the region $16 < y/l_H < 32$, the joint p.d.f. of the topologies shows a similar distribution to buffer layers and also the extents are the largest.

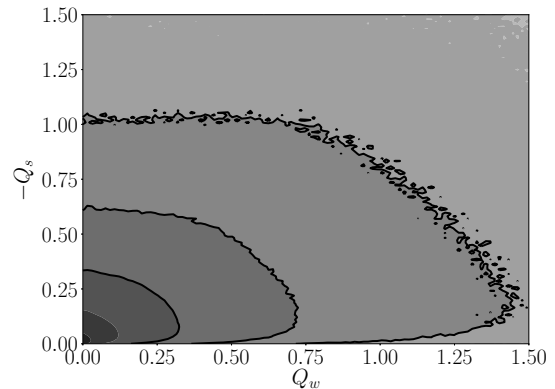
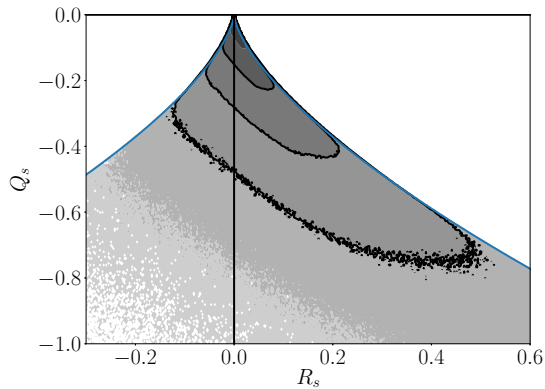
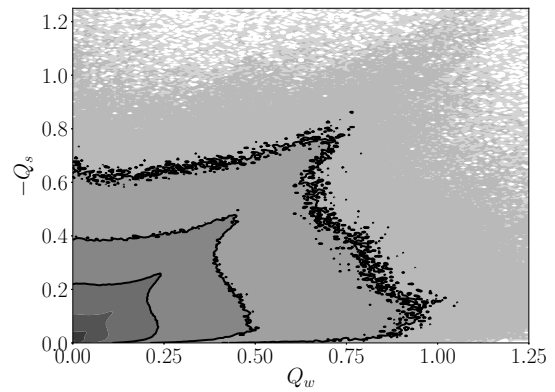
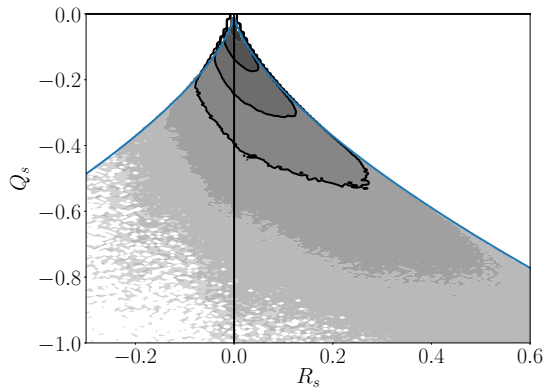
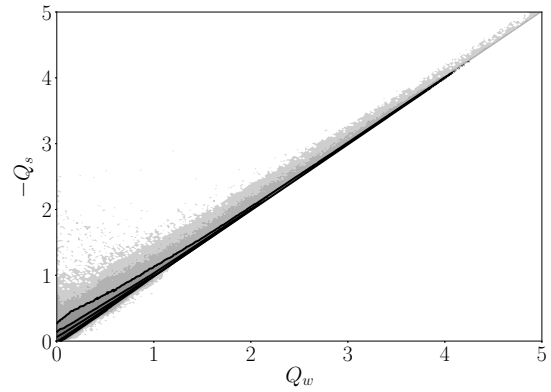
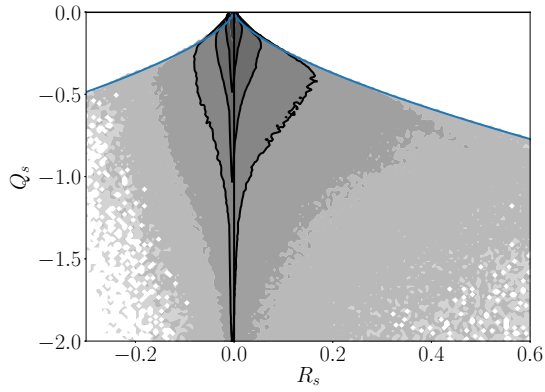


Figure 7. Joint Probability density function between Q_s and R_s normalized by $\langle Q_w \rangle_V$ in the regions $0 < y/l_H < 1$, $1 < y/l_H < 16$ and $16 < y/l_H < 32$.

Figure 8. Joint Probability density function between Q_s and Q_w normalized by $\langle Q_w \rangle_V$ in the regions $0 < y/l_H < 1$, $1 < y/l_H < 16$ and $16 < y/l_H < 32$.

ACKNOWLEDGEMENT

This research is supported by the ARC which is gratefully acknowledged. The computational facilities supporting this project include the Australian NCI National Facility, Pawsey Supercomputing Centre and the Multi-modal Australian Sciences Imaging and Visualisation Environment (MASSIVE), which were provided by an NCMAS grant.

REFERENCES

Blackburn, Hugh M, Mansour, Nagi N & Cantwell, Brian J 1996 Topology of fine-scale motions in turbulent channel flow. *Journal of Fluid Mechanics* **310**, 269–292.
 Chong, MS, Soria, J, Perry, AE, Chacin, J, Cantwell, BJ &

Na, Y 1998 Turbulence structures of wall-bounded shear flows found using dns data. *Journal of Fluid Mechanics* **357**, 225–247.
 Chong, Min S, Perry, Anthony E & Cantwell, Brian J 1990 A general classification of three-dimensional flow fields. *Physics of Fluids A: Fluid Dynamics* **2** (5), 765–777.
 Coleman, GN, Pirozzoli, S, Quadrio, Maurizio & Spalart, PR 2017 Direct numerical simulation and theory of a wall-bounded flow with zero skin friction. *Flow, Turbulence and Combustion* **99** (3-4), 553–564.
 Kim, John, Moin, Parviz & Moser, Robert 1987 Turbulence statistics in fully developed channel flow at low reynolds number. *Journal of fluid mechanics* **177**, 133–166.
 Sekimoto, Atsushi, Atkinson, Callum & Soria, Julio 2018 Characterisation of minimal-span plane couette turbu-

- lence with pressure gradients. In *Journal of Physics: Conference Series*, , vol. 1001, p. 012020. IOP Publishing.
- Sekimoto, Atsushi, Dong, Siwei & Jiménez, Javier 2016a Direct numerical simulation of statistically stationary and homogeneous shear turbulence and its relation to other shear flows. *Physics of Fluids* **28** (3), 035101.
- Sekimoto, A., Kitsios, V., Atkinson, C., Jimenez, J. & Soria, J. 2016b Coherent structures in a self-similar adverse pressure gradient turbulent boundary layer. In *Proceedings of the 20th Australasian Fluid Mechanics Conference (AFMC)*. Australia: Australasian Fluid Mechanics Society.
- da Silva, Carlos B & Pereira, José CF 2008 Invariants of the velocity-gradient, rate-of-strain, and rate-of-rotation tensors across the turbulent/nonturbulent interface in jets. *Physics of fluids* **20** (5), 055101.
- Soria, J, Ooi, A & Chong, MS 1997 Volume integrals of the qa-ra invariants of the velocity gradient tensor in incompressible flows. *Fluid dynamics research* **19** (4), 219–233.
- Soria, J, Sondergaard, R, Cantwell, BJ, Chong, MS & Perry, AE 1994 A study of the fine-scale motions of incompressible time-developing mixing layers. *Physics of Fluids* **6** (2), 871–884.
- Stratford, BS 1959 The prediction of separation of the turbulent boundary layer. *Journal of fluid mechanics* **5** (1), 1–16.